Genes & Diseases (2023) 10, 1641–1656

Available online at www.sciencedirect.com

ScienceDirect

journal homepage: www.keaipublishing.com/en/journals/genes-diseases

FULL LENGTH ARTICLE

Suppression of osteosarcoma progression by engineered lymphocyte-derived proteomes

Kexin Li [a,b], Xun Sun [a,b], Hudie Li [a,b], Hailan Ma [a,b], Meng Zhou [a,b], Kazumasa Minami [c], Keisuke Tamari [c], Kazuhiko Ogawa [c], Pankita H. Pandya [d,e], M. Reza Saadatzadeh [d,e], Melissa A. Kacena [d,f,g], Karen E. Pollok [d,e], Bai-Yan Li [a,**], Hiroki Yokota [b,d,g,*]

[a] *Department of Pharmacology, School of Pharmacy, Harbin Medical University, Harbin, Heilongjiang 150081, China*
[b] *Department of Biomedical Engineering, Indiana University Purdue University Indianapolis, Indianapolis, IN 46202, USA*
[c] *Department of Radiation Oncology, Osaka University Graduate School of Medicine, Suita, Osaka 565-0871, Japan*
[d] *Simon Comprehensive Cancer Center, Indiana University School of Medicine, Indianapolis, IN 46202, USA*
[e] *Department of Pediatrics, Indiana University School of Medicine, Indianapolis, IN 46202, USA*
[f] *Department of Orthopaedic Surgery, Indiana University School of Medicine, Indianapolis, IN 46202, USA*
[g] *Indiana Center for Musculoskeletal Health, Indiana University School of Medicine, Indianapolis, IN 46202, USA*

Received 16 April 2022; accepted 12 August 2022
Available online 28 August 2022

KEYWORDS
Calreticulin;
Lymphocytes;
Moesin;
Osteosarcoma;
PKA;
Proteome

Abstract Cancer cells tend to develop resistance to chemotherapy and enhance aggressiveness. A counterintuitive approach is to tame aggressiveness by an agent that acts opposite to chemotherapeutic agents. Based on this strategy, induced tumor-suppressing cells (iTSCs) have been generated from tumor cells and mesenchymal stem cells. Here, we examined the possibility of generating iTSCs from lymphocytes by activating PKA signaling for suppressing the progression of osteosarcoma (OS). While lymphocyte-derived CM did not present anti-tumor capabilities, the activation of PKA converted them into iTSCs. Inhibiting PKA conversely generated tumor-promotive secretomes. In a mouse model, PKA-activated CM suppressed tumor-

* Corresponding author. Department of Biomedical Engineering, Indiana University Purdue University Indianapolis, Indianapolis, IN 46202, USA.
** Corresponding author.
E-mail addresses: liby@ems.hrbmu.edu.cn (B.-Y. Li), hyokota@iupui.edu (H. Yokota).
Peer review under responsibility of Chongqing Medical University.

https://doi.org/10.1016/j.gendis.2022.08.007

induced bone destruction. Proteomics analysis revealed that moesin (MSN) and calreticulin (Calr), which are highly expressed intracellular proteins in many cancers, were enriched in PKA-activated CM, and they acted as extracellular tumor suppressors through CD44, CD47, and CD91. The study presented a unique option for cancer treatment by generating iTSCs that secret tumor-suppressive proteins such as MSN and Calr. We envision that identifying these tumor suppressors and predicting their binding partners such as CD44, which is an FDA-approved oncogenic target to be inhibited, may contribute to developing targeted protein therapy.

Introduction

In response to chemotherapeutic agents, cancer cells tend to develop resistance, for any action can induce an opposite reaction in mechanics. Cancer cells also enhance their aggressiveness as the natural selection law entails a survival of the fittest. In developing a novel option for cancer treatment, we developed an unconventional approach that would consider the reactive mechanism as well as competition among cells. In this study, we reported the use of activating oncogenic signaling instead of inactivating it and converting oncogenic signaling into anti-oncogenic signaling using engineered lymphocytes for osteosarcoma (OS) as a cancer model.

OS is the most common type of primary bone cancer, usually occurring in the lower limb of children and adolescents.[1] While the primary therapeutic regimen is surgery combined with adjuvant chemotherapy and the current standard-of-care MAP therapy using methotrexate, doxorubicin, and cisplatin has saved many lives, the prognosis of the metastatic or recurrent OS remains high.[2,3] Pathways such as Wnt, PI3K, RANKL, and Notch have been implicated in OS pathobiology,[4] but few recurrent targetable mutations have been identified and the efficacy of immunotherapy is controversial.[5] To build a novel therapeutic option, we examined the administration of a conditioned medium (CM) by generating induced tumor-suppressing cells (iTSCs).[6] The formation of iTSCs requires a counterintuitive approach in which tumorigenic signaling such as Wnt, PI3K, and EMT induction is activated for producing tumor-suppressive proteomes.[7–9] Our previous studies have shown that the activation of Wnt and PI3K signaling in bone cells such as osteocytes, osteoblasts, and MSCs as well as solid cancer cells including breast, prostate, and pancreatic cancer cells can convert those cells into iTSCs.[10–14] For instance, the overexpression of *β-catenin* in osteocytes and *Akt* in MSCs made their CM anti-oncogenic, and the administration of their CMs inhibited the growth of mammary tumors and tumor-driven bone degradation.[10–12]

While bone marrow-derived MSCs have attracted attention in regenerative medicine because of their differentiation capacity and immunomodulatory properties, blood-derived mononuclear cells and lymphocytes have also been placed on center stage in translational medicine.[15] CAR T-cell immunotherapy, for instance, is an excellent example of the use of engineered T cells to fight against cancer.[16] This study described another engineering procedure to convert lymphocytes into cancer-fighting cells, using OS, rare cancer mostly for children, as a model system. Effective drugs, directed to the treatment of OS, have not been developed for the last 40 years.[17] This study aimed to explore the use of peripheral blood for a novel therapeutic option of OS, focusing on lymphocyte-derived CM.

Regarding the generation of iTSCs not only from non-cancer cells but also from cancer cells, an intriguing question is the mechanism of inducing tumor-suppressive CM by activating tumorigenic signaling. Cancer cell secretomes are generally considered tumorigenic[18] since they contribute to building a tumor microenvironment and inducing chemoresistance.[19] Besides soluble factors such as interleukins, cytokines, growth factors, and other metabolites, the secretomes also contain exosomes with oncogenic RNAs.[20] On the contrary, one caution is context dependence in interpreting the role of secretomes. Our group has shown that proteins such as a heat shock protein, Hsp90ab1, act as a tumor promoter intracellularly and a tumor suppressor extracellularly.[12] Others also have shown that high mobility group box protein 1 (HMGB1) serves as a cytoplasmic tumor suppressor and an extracellular tumor promoter.[21] Thus, tumorigenic factors in the cytoplasm may deceitfully act as tumor-suppressive factors in the secretome. Furthermore, another observation is the induction of chemoresistance by the administration of chemotherapeutic agents. If any tumor-inhibitory agents may induce tumor-promotive secretomes,[22] a rational, counterintuitive approach is to generate tumor-suppressive secretomes by applying tumor-promotive agents.

The concept of iTSCs also arose from the biological cell competition observed during Drosophila organogenesis as well as mouse embryogenesis.[23,24] Briefly, in the formation of Drosophila wing discs, cells with higher protein synthesis are reported to eliminate neighboring cells with lower protein synthesis. Likewise, in mouse embryos, it is also reported that cells with lower Myc levels are removed by apoptosis, and cells with higher Myc levels proliferate to fill the vacant spaces.[25] These mechanisms indicate the possibility of removing tumor cells by generating highly metabolically active cells. While a hallmark of tumor cells is uncontrolled growth,[26] many lines of evidence in our previous studies demonstrate that the activation of Wnt and PI3K signaling in tumor cells and non-tumor cells generate tumor-suppressive secretomes. This paradoxical approach of activating cell-proliferating signalings has been shown effective for solid tumors including breast,

prostate, and pancreatic cancers, although the efficacy of anti-tumor actions differs depending on the type of iTSC-generating cell and their activated pathways.[10–14] Because of the accessibility of patient-derived peripheral blood, we herein focused on converting lymphocytes into iTSCs. The preliminary screening of cell-proliferating signaling revealed that the activation of PKA signaling[27] is effective for generating iTSCs from lymphocytes, as compared to activation of Wnt and PI3K signaling.[6]

PKA is commonly known as a cAMP-dependent protein kinase, which is activated by the binding of cAMP and phosphorylates numerous metabolic enzymes.[28] Since the activation of PKA generally produces metabolically active cells, the question addressed in this study was whether PKA-activated lymphocytes become iTSCs and generate CM that can inhibit the progression of osteosarcoma *in vitro* and *in vivo* (PKA CM). To determine the regulatory mechanism underlying this counterintuitive approach of activating PKA signaling as a cancer therapy, we examined the contribution of two known tumor suppressors, moesin (MSN)[29] and calreticulin (Calr),[30] since these two proteins in the extracellular domain were shown to act as tumor-suppressing proteins in our previous iTSC studies.[12,13] We have previously reported that extracellular MSN acts as a tumor suppressor by interacting with CD44 that drives aggressiveness and chemoresistance of metastatic OS.[13,31]

To begin to evaluate the downstream effectors that may mediate the anti-tumor action of extracellular Calr, we completed immunoprecipitation assays. Specifically, Calr immunoprecipitated CD91, a signaling receptor to prime immune responses of T cells and macrophages,[32] as well as CD47, an immunoglobulin that is reported to be overexpressed on the surface of many types of cancer cells.[33] Collectively, this study revealed the potent anti-tumor effects of PKA-activated lymphocytes, which are in part mediated by the Calr-CD47/CD91 axis. It also indicated the possibility of developing a unique proteome-based therapy, as well as the identification of cell-surface receptors as druggable targets that should mediate the anti-tumor actions of iTSCs and their CM.

Materials and methods

Cell culture and agents

MG63 human OS cells and U2OS human OS cells (Sigma, St. Louis, MO, USA) were cultured in DMEM. Jurkat T lymphocytes were cultured in RPMI1640.[34] Primary human T lymphocytes (#33002-02, Celprogen, CA, USA) were cultured in CTS™ OpTmizer™ T-Cell Expansion SFM (#A3705001, Thermo Fisher Scientific, Waltham, MA, USA). MLO-A5 osteocyte-like cells (obtained from Dr. L. Bonewald, Indiana University, IN, USA), RAW264.7 pre-osteoclast cells (ATCC, Manassas, VA, USA),[35] and MC3T3 osteoblasts (Sigma) were grown in αMEM. Patient-derived xenograft (PDX) xenoline (TT2-77) were grown in DMEM.[36] Human mesenchymal stem cells (MSCs) (Lonza, Basel, Switzerland) were grown in MSCBM (Lonza). The culture media were supplemented with 10% FBS (fetal bovine serum) and antibiotics (penicillin and streptomycin), and cells were maintained at 37°C and 5% CO_2.

MSN (1 μg/mL, MBS2031729, MyBioSource, San Diego, California, USA), and Calr (0.7 μg/mL, MBS2009125) recombinant proteins were given to U2OS cells, and cells were incubated for 24 h. A PKA signaling activator (CW008, 20 μM and 50 μM, #5495, Tocris, Minneapolis, MN, USA)[37] and an inhibitor of PKA signaling (H89 dihydrochloride, 20 μM, #2910, Tocris)[38] were applied to the cells for 24 h. Cyclic AMP (10 μM, 50 μM and 100 μM, #A23811G, Thermo Fisher Scientific) and Dibutyryl cAMP (100 μM, 200 μM and 500 μM, #1141, Tocris) were applied to the cells for 24 h.

Preparation of conditioned medium (CM)

For *in vitro* experiments, CM was subjected to low-speed centrifugation at 2,000 rpm for 10 min. The cell-free supernatants were centrifuged at 4,000 rpm for 10 min and subjected to filtration with a 0.22-μm polyethersulfone membrane (Sigma). For examining the efficacy of CM *in vivo*, fetal bovine serum-free CM was condensed by a filter with a cutoff molecular weight of 3 kDa and the 10-fold condensed CM (50 μL re-suspended in PBS) was intravenously injected from the tail vein.

Generating the CM from human peripheral blood

The study with human peripheral blood samples was conducted according to the guidelines of the Declaration of Helsinki and approved by the ethics committee of Osaka University (protocol #21344). We collected 8 mL peripheral blood from 4 healthy volunteers (mean of 33 years, ranging from 22 to 64 years) into a blood collection tube (#362753, Becton, Dickinson and Company, NJ, USA). Blood samples were diluted by the addition of an equal volume of 0.9% NaCl solution. In a 15 mL centrifuge tube, 3 mL of Lymphoprep™ (# 1,114,544, Abbott Diagnostics Technologies AS, Norway) was added onto 6 mL of the diluted blood sample. Samples were centrifuged at 800 × *g* for 30 min at room temperature. After centrifugation, the mononuclear cell fractions were collected with a Pasteur pipette. The harvested fractions were cultured in AlyS705 medium (Cell Science & Technology Institute, Inc., JAPAN) and CW008 (50 μM) was added. After 24 h, the culture medium was changed to a fresh medium, and CW008 was completely removed. The cells were incubated for 24 h. The supernatant of the culture medium was collected and centrifuged (1,000 × *g* for 10 min, 14,000 × *g* for 2 min, and 14,000 × *g* for 60 min) to separate the CM. The CM was further concentrated to ~10-fold by a centrifugal evaporator (Genevac EZ-2 Plus, SP Scientific, NY, USA). The final protein concentration was adjusted to 0.23 μg/μL.

Human lymphocyte separation

Lymphocytes were isolated using a lymphocyte separation medium (LSM, Corning, Glendale, Arizona, USA). In brief, a blood sample (3W-902, Lonza) was diluted with an equal volume of RPMI1640, and 4 mL of diluted blood sample were carefully layered (not mixed) on top of 3 mL of LSM. The mixture was centrifuged at 400 × *g* for 30 min at room temperature. The lymphocyte layer was transferred to a new tube, and cells were diluted with 5 volumes of RPMI1640. They were mixed gently and centrifuged at 500

× *g* for 10 min. A cell pellet was rinsed 2 times with PBS, and the final pellet was re-suspended in RPMI1640. Harvested cells were mononuclear cells that included lymphocytes and monocytes.

MTT and EdU assays

MTT-based metabolic activity was evaluated using 2,000−3,000 OS cells seeded in 96-well plates (Corning). CM was given on day 2, and OS cells were dyed with 0.5 mg/mL thiazolyl blue tetrazolium bromide (Sigma) on day 4 for 4 h. Optical density for assessing metabolic activities was determined at 570 nm using a multi-well spectrophotometer.

Using the EdU procedure previously described,[39] cellular proliferation was examined using a fluorescence-based cell proliferation kit (Click-iT™ EdU Alexa Fluor™ 488 Imaging Kit; Thermo Fisher Scientific). Approximately 1,000 cells were seeded in 96-well plates (Corning) on day 1, CM was given on day 2, and cells were labeled with 10 μM EdU on day 4 for 4 h. After labeling, cells were fixed in a 3.7% (w/v) formaldehyde solution for 15 min at room temperature. Cells were washed with a PBS buffer (3% BSA, 0.5% Triton® X-100) and incubated with a freshly prepared Click-iT® reaction cocktail in dark for 30 min. After rinsing with a PBS buffer, at least four images from four wells in each group were taken with a fluorescence microscope (magnification, 100 × , Olympus, Tokyo, Japan). The number of fluorescently labeled cells, as well as the total number of cells, were counted using Image *J* (National Institutes of Health, Bethesda, MD, USA) and the ratio of the fluorescently labeled cells to the total cells was determined.

Transwell invasion and scratch motility assays

The invasion capacity of OS cells was determined using a 12-well plate and transwell chambers (Thermo Fisher Scientific) with 8-μm pore size. Transwell chambers were coated with 300 μL Matrigel (100 μg/mL) that was polymerized and dried overnight. 500 μL of the serum-free medium was added to each chamber and after 1 h, the chamber was washed three times with the serum-free medium. Approximately 7×10^4 cells in 300 μL serum-free DMEM were then placed in the upper chamber and 800 μL CM was added to the lower chamber. After 48 h, the cells on the upper surface of the membrane were removed and the membrane was treated with ∼400 μL of 75% ethanol in a fresh 12-well plate for 40 min. The cells, which invaded the lower side of the membrane, were stained with Crystal Violet (diluted 1:25 in water) for 30 min. At least five randomly chosen images were taken with an inverted optical microscope (magnification, 100 × , Nikon, Tokyo, Japan), and the average number of stained cells, which represented the invasion capacity, was determined.

A wound-healing scratch motility assay was performed to assess 2-dimensional cell motility. Approximately 4×10^5 cells were seeded in 12-well plates, and after the cell attachment, a scratch was made on the cell layer with a plastic pipette tip. Cell medium was exchanged and floating cells were removed. Images of the cell-free areas were captured at 0 h and 24 h after scratching via an inverted microscope with a magnification of 40 × . The areas of 4 images in each group were quantified with Image J.[40]

Cell co-culturing assay

Fluorescently labeled U2OS cells were prepared by culturing them with green fluorescent dyes (4705, Sartorius, Gottingen, Germany) for 20 min at 37°C. Approximately 2000 fluorescently labeled U2OS cells were cultured in a 96-well plate (Corning) with or without normal RAW264.7 cells in complete DMEM (10% FBS, 1% antibiotics). Five images for each group were captured with a fluorescence microscope (magnification, 100 × , Olympus) at 0 and 24 h and evaluated with Image *J*.

Western blot analysis and ELISA assay

Cells were lysed in a radio-immunoprecipitation assay buffer with protease inhibitors (PIA32963, Thermo Fisher Scientific) and phosphatase inhibitors (2,006,643, Calbiochem, Billerica, MA, USA). After cell lysis, proteins were fractionated by 10%−15% SDS gels and electro-transferred to polyvinylidene difluoride transfer membranes (IPVH00010, Millipore, Billerica, MA, USA). After blocking 1 h with a blocking buffer (1,706,404, Bio-Rad, Hercules, CA, USA), the membrane was incubated overnight with primary antibodies and then with secondary antibodies conjugated with horseradish peroxidase for 45 min (7074 S/7076 S, Cell Signaling, Danvers, MA, USA). We used antibodies against Lrp5, Runx 2, Snail, MSN, Calr, cleaved-caspase 3, caspase 3, CD91, p-CREB, and CREB (Cell Signaling), c-fos, NFATc1, Cathepsin K (Santa Cruz Biotechnology, Dallas, TX, USA), CD47 (Thermo Fisher Scientific), Collagen I (Novus Biologicals, CO, USA), Osteocalcin (abcam, Boston, MA, USA), and β-actin as a control (A5441, Sigma). The protein level was determined using a SuperSignal west femto maximum sensitivity substrate (PI34096, Thermo Fisher Scientific), and a luminescent image analyzer (LAS-3000, Fuji Film, Tokyo, Japan) was used to quantify signal intensities.[41] The levels of Calr and MSN in CW008-treated CM were determined using the ELISA kits (MBS263181 and MBS2709503; MyBioSource).

RNA interference

RNA interference with specific siRNAs was conducted to silence *CD91* (106,762) and *CD47* (145,977, Thermo Fisher Scientific), together with nonspecific negative control siRNAs (Silencer Select #1, Thermo Fisher Scientific). Cells were transiently transfected with siRNA using Lipofectamine RNAiMAX (13,778,075, Life Technologies). The medium was replaced by a regular culture medium after 24 h, and the efficiency of silencing was assessed with immunoblotting 24 h after transfection.

Immunoprecipitation

Immunoprecipitation was conducted with an immunoprecipitation starter pack kit (Cytiva, Marlborough, MA, USA), using the procedure the manufacturer provided. In brief, 20 μL of protein A sepharose was washed twice with PBS and incubated with 2 μg of antibodies for Calr. In parallel, normal IgG was prepared for negative control. We employed two kinds of protein samples, including RAW264.7 cell lysate, as well as U2OS cell lysate. The antibody-cross-linked beads

were incubated overnight with 600 μL protein samples on a shaker. The beads were collected by centrifugation, washed three times with PBS, and resuspended for Western blotting. The protein samples before the immunoprecipitation were used as positive controls. Western blotting was conducted using antibodies against Calr, CD91, and CD47.

Differentiation of osteoblasts and osteoclasts

The differentiation assay of RAW264.7 pre-osteoclasts was performed in a 12-well plate. During the 6-day incubation of pre-osteoclast cells with 40 ng/mL of RANKL, the culture medium was exchanged once on day 4. Adherent cells were fixed and stained with a tartrate-resistant acid phosphate (TRAP)-staining kit (Sigma), according to the manufacturer's instructions. TRAP-positive multinucleated cells (>3 nuclei) were identified as mature osteoclasts.[42] To evaluate the effect of CW CM on the differentiation of osteoblasts, MC3T3 osteoblasts were cultured in the osteogenic medium that consisted of 50 μg/mL ascorbic acid and 5 mM sodium β-glycerophosphate with 10% FBS and antibiotics. The medium was exchanged every 3 days and cells were fixed and stained with Alizarin red to visualize calcium deposits in 4 weeks.[43]

Animal model

The experimental procedures using animals were approved by the Indiana University Animal Care and Use Committee and were complied with the Guiding Principles in the Care and Use of Animals endorsed by the American Physiological Society. Mice were housed five per cage and provided with mouse chow and water *ad libitum*. In the mouse model of osteolysis (3 groups, 8 mice per group, ~8 weeks), NOD/SCID/γ (−/−) (NSG) mice received an injection of U2OS cells (2.5×10^5 cells in 20 μL PBS), into the right tibia as an intra-tibial injection. The three treatment groups were 1) placebo, 2) Jurkat-derived CM without CW008 treatment, and 3) Jurkat-derived CM with CW008 treatment. CM was given daily as an intravenous injection to the tail vein. Mice were sacrificed after 18 days and the hindlimbs were harvested for microCT imaging and histology.

X-ray

Whole-body X-ray imaging was performed using a Faxitron radiographic system (Faxitron X-ray Co., Tucson, AZ, USA).[44] Tibial integrity was scored in a blinded manner on a scale of 0−3: 0 = normal with no indication of a tumor, 1 = clear bone boundary with slight periosteal proliferation, 2 = bone damage and moderate periosteal proliferation, and 3 = severe bone erosion.

microCT imaging and histology

The tibiae were harvested for micro-computed tomography (μCT) imaging and histology. μCT was performed with Skyscan 1172 (Bruker-MicroCT, Kontich, Belgium).[45] Scans were performed at pixel size 8.99 μm and the images were reconstructed (nRecon v1.6.9.18) and analyzed (CTan v1.13). Using μCT images, trabecular bone parameters such as bone volume ratio (BV/TV), bone mineral density (BMD), trabecular number (Tb.*n*), and trabecular separation (Tb.Sp) were determined in a blinded fashion. For histology, H&E staining was conducted as described previously.[46] Of note, normal bone cells appeared as a regular shape with round and deeply stained nuclei, while tumor cells were of a distorted shape with irregularly stained nuclei.

Statistical analysis

For cell-based experiments, three or four independent experiments were conducted and data were expressed as mean ± S.D. Statistical significance was evaluated using a one-way analysis of variance (ANOVA). Post hoc statistical comparisons with control groups were performed using Bonferroni correction with statistical significance at $P < 0.05$. In animal experiments, we employed 8 mice per group to obtain statistically significant differences in bone volume ratio as a primary outcome measure. The single and double asterisks in the figures indicate $P < 0.05$ and $P < 0.01$, respectively.

Ethics statement

All animal experiments were conducted according to protocols approved by the Indiana University Animal Care and Use Committee and were complied with the Guiding Principles in the Care and Use of Animals endorsed by the American Physiological Society (protocol #330R). The study with human peripheral blood samples was conducted according to the guidelines of the Declaration of Helsinki and approved by the ethics committee of Osaka University (protocol #21344).

Results

Suppression of tumorigenic behaviors of U2OS cells by CW008-treated jurkat cell-derived CM

Using a PKA activator (20 μM of CW008), we generated CW008-treated T-cell derived CM (CW CM) with Jurkat T-lymphocytes. Notably, CW CM suppressed MTT-based viability in 2 days, scratch-based migration in 1 day, EdU-based proliferation in 2 days, and transwell invasion in 2 days of the OS cell line, U2OS cells (Fig. 1A−D). The suppression of the viability, migration, and proliferation was validated in another OS cell line, MG63 cells (Fig. 1E−G). To evaluate the degree of unwanted elimination of non-tumor cells, we defined a tumor-selectivity factor, λ, using MTT-based metabolic activities. Since λ is defined as the ratio of (MTT reduction in tumor cells) to (MTT reduction in non-tumor cells), the value of λ above 1 indicates that an inhibitory effect is tumor-selective. We observed that the inhibitory effect of CW CM was tumor-selective and stronger in two OS cell lines than bone cells such as MSCs and an osteocyte cell line, MLO-A5 cells (Fig. S1). By contrast, we observed the opposite pro-tumor effect by a PKA inhibitor, H89 dihydrochloride. H89-treated Jurkat-derived CM (H89 CM) promoted MTT-based viability in 2

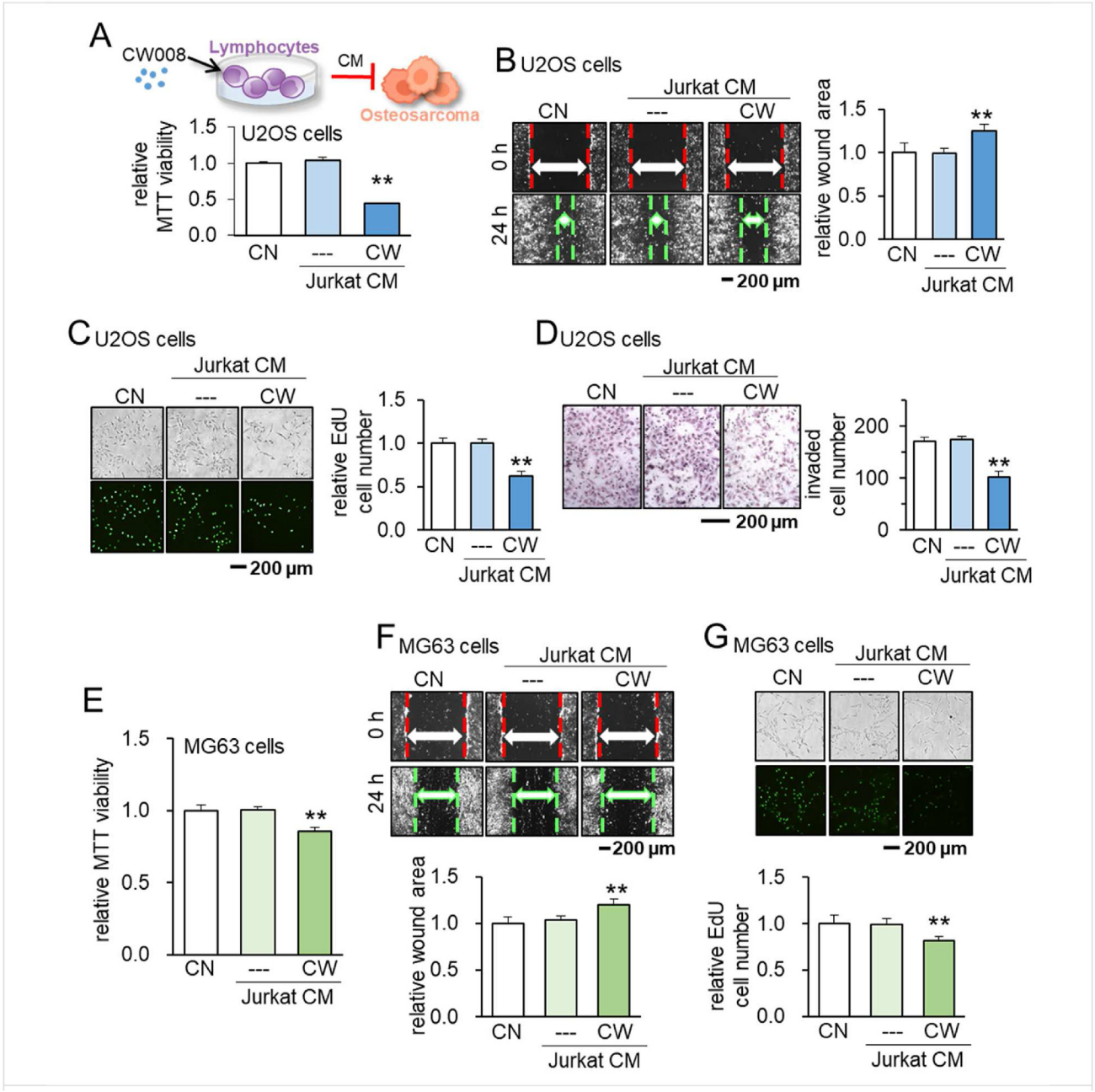

Figure 1 Suppression of tumorigenic behaviors of U2OS and MG63 OS cells by CW008-treated Jurkat cell-derived CM. CN = control, CW = CW008, and CM = conditioned medium. The double asterisk indicates $P < 0.01$ **(A—D)** Schematic illustration of CW008-treated Jurkat cell-derived CM generation, and suppression of MTT-based viability, scratch-based migration, EdU-based proliferation, and transwell invasion of U2OS cells by CW008-treated Jurkat cell-derived CM, respectively. **(E—G)** Suppression of MTT-based viability, scratch-based migration, and EdU-based proliferation of MG63 OS cells by CW008-treated Jurkat cell-derived CM, respectively.

days, EdU-based proliferation in 2 days, and transwell invasion in 2 days in U2OS cells (Fig. S2A—C), as well as MG63 cells (Fig. S2D—F).

Tumor-suppressive effects of cAMP-treated CM

To further evaluate the anti-tumor effect of PKA-activated lymphocyte proteomes, we evaluated the response to cAMP and cAMP analog using Jurkat cells as well as primary human lymphocytes. Jurkat-derived CM after the treatment with cAMP and D-cAMP inhibited MTT-based viability in 2 days in U2OS and/or MG63 cells (Fig. 2A—C). Consistently, cAMP treated Jurkat-derived CM suppressed EdU-based proliferation, and transwell invasion in 2 days in U2OS cells (Fig. 2D, E). Besides Jurkat cells, primary human T lymphocyte-derived CW008-treated CM suppressed MTT-based viability of U2OS and MG63 cells (Fig. 2F, G). Of note,

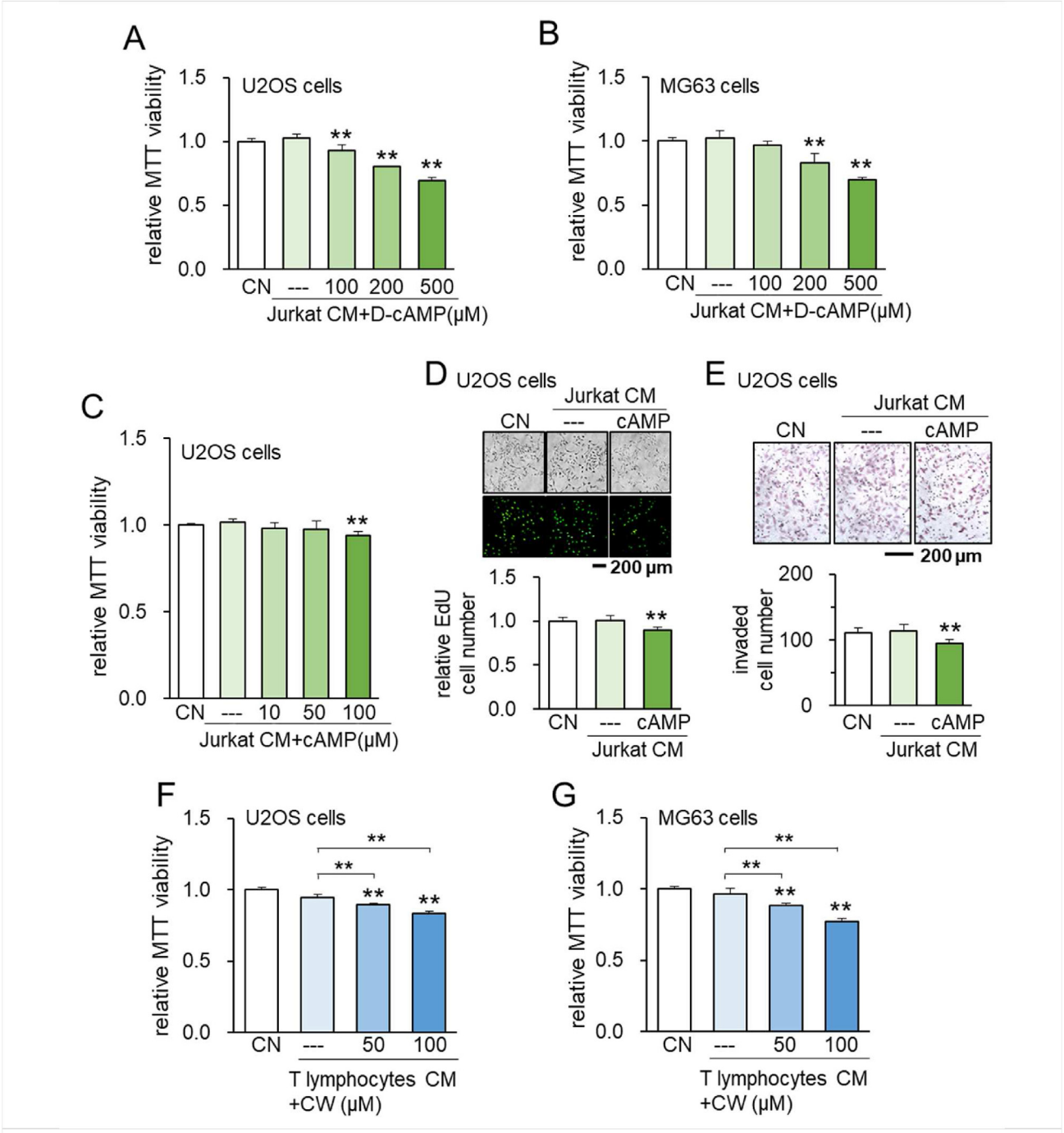

Figure 2 Suppression of tumorigenic behaviors of U2OS and MG63 OS cells by D-cAMP/cAMP- treated Jurkat cell-derived CM. CN = control, D-cAMP = Dibutyryl cAMP, CW = CW008, and CM = conditioned medium. The double asterisk indicates $P < 0.01$. **(A, B)** Suppression of MTT-based viability of U2OS and MG63 OS cells by D-cAMP-treated Jurkat cell-derived CM, respectively. **(C—E)** Suppression of MTT-based viability, EdU-based proliferation, and transwell invasion of U2OS cells by cAMP-treated Jurkat cell-derived CM. **(F, G)** Suppression of MTT-based viability of U2OS and MG63 OS cells by CW008-treated primary human T lymphocyte-derived serum-free CM, respectively.

we observed the elevation in p-CREB, cAMP-response element-binding protein, in Jurkat cells in 1 day by the administration of CW008 (Fig. S3). Collectively, the data suggest that activation of PKA signaling in lymphocytes promotes the anti-tumor capabilities of lymphocyte-derived CM.

Tumor-suppressive capability of MSC- and osteoblast-derived CM

To examine the possibility of generating iTSCs from other types of cells, we employed MSCs and osteoblasts. The result showed that CW008-treated MSC-derived CM

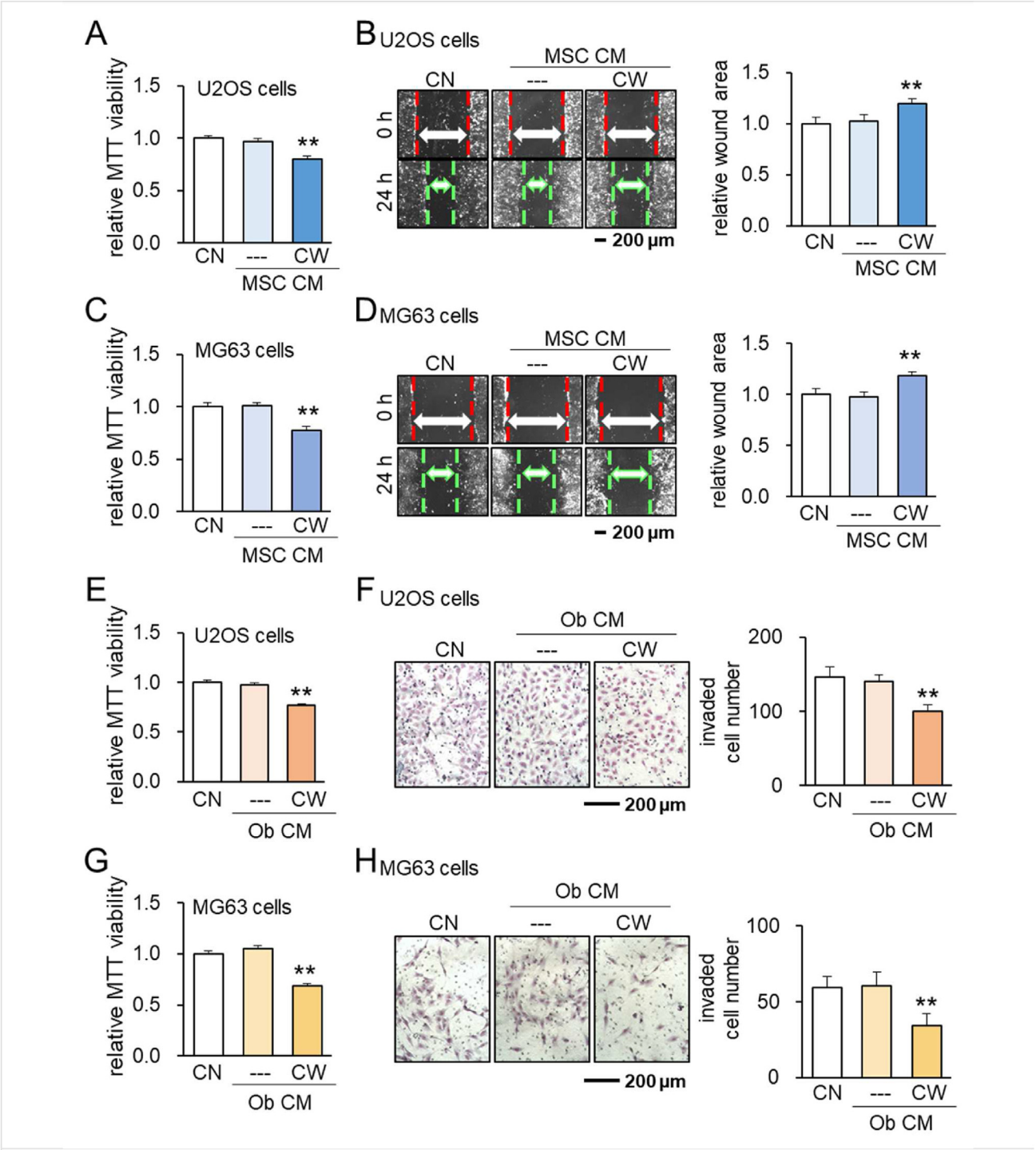

Figure 3 Suppression of tumorigenic behaviors of U2OS and MG63 OS cells by CW008-treated MSC cell-derived CM and CW008-treated MC3T3 osteoblast cell-derived CM. CN = control, CW = CW008, Ob = osteoblast, and CM = conditioned medium. The double asterisk indicates $P < 0.01$. **(A—D)** Suppression of MTT-based viability and scratch-based migration of U2OS and MG63 OS cells by CW008-treated MSC cell-derived CM, respectively. **(E—H)** Suppression of MTT-based viability and transwell invasion of U2OS and MG63 OS cells by CW008-treated osteoblast cell-derived CM, respectively.

inhibited MTT-based viability and scratch-based migration in U2OS cells (Fig. 3A, B) and MG63 cells (Fig. 3C, D). The same anti-tumor responses were also observed with CW008 treated-osteoblast derived-CM for U2OS cells (Fig. 3E , F) as well as MG63 cells (Fig. 3G, H). Taken together, the result supported the notion that anti-tumor CM can be derived from T lymphocytes, MSCs, and osteoblasts by the treatment with CW008.

Inhibition of osteoclast differentiation, stimulation of osteoblast differentiation, and prevention of bone loss *in vivo*

So far, we have observed the suppression of *in vitro* OS progression by PKA-activated cell-derived CM. Since osteoclasts and osteoblasts play a critical role in bone metabolism, we next examined the effect of PKA-activated CM on the differentiation of RAW264.7 pre-osteoclasts and MC3T3 osteoblasts. In response to lymphocyte-derived CW CM, RANKL-stimulated RAW264.7 cells reduced the number of TRAP-positive and multi-nucleated cells in 5 days (Fig. 4A—C). Consistently, CW CM downregulated c-fos, a key regulator of osteoclast-macrophage lineage determination and bone remodeling, and NFATc1, a master transcription factor for osteoclast differentiation, together with Cathepsin K, a cysteine proteinase largely responsible for the degradation of bone matrix (Fig. 4D). By contrast, we observed the opposite action on the osteoclast differentiation in response to H89 CM (Fig. 4A—D). Regarding the effect on bone-forming osteoblasts, the culturing of MC3T3 cells in CW CM increased Alizarin red staining, a measure of calcium deposition and osteoblast differentiation, in 4 weeks (Fig. 4E, F). CW CM also elevated the level of type I collagen in MSCs and osteocalcin in MC3T3 cells for 7 days in the presence and absence of 50 μg/mL ascorbic acid and 5 mM β-glycerophosphate (Fig. S4).

Bone protection *in vivo* by CW CM

Next, using an intratibial OS mouse model whereby U2OS cells were injected, daily administration of CW CM for 18 days significantly reduced tumor-induced trabecular bone loss or osteolysis (Fig. 5A—C). The increase in the bone volume ratio, bone mineral density, and the trabecular number was in agreement with the suppression of the tumor-invaded area in the proximal tibia in the H&E-stained bone sections (Fig. S5). Of note, the tumor-invaded area presented irregular-shaped spaces with a fewer number of bone marrow cells. Collectively, this suggests that the systemic administration of CW CM can protect bone, possibly by the inhibition of tumor progression but also by directly regulating the function of osteoclasts and osteoblasts.

Anti-tumor effects of peripheral blood-derived CM

Besides Jurkat cells, we examined the anti-tumor effects of CM that were derived from lymphocytes and mononuclear cells using human peripheral blood samples. Specifically, lymphocytes were isolated using a lymphocyte isolation kit, while mononuclear cells, which contained lymphocytes and monocytes, were isolated by a density gradient centrifugation. Isolated cells were treated with 50 μM CW008 for 1 day and the collected CM was condensed by 10 times. The result showed that CW008-treated lymphocyte-derived CM inhibited MTT-based viability and transwell invasion of MG63 and U2OS cells (Fig. 6A—D). This anti-tumor effect was observed with mononuclear cells prepared from four separate human peripheral blood samples (Fig. 6E, F).

Moesin (MSN) and calreticulin (Calr) as tumor-suppressing proteins

We next began to determine the mechanism of anti-tumor actions by focusing on MSN and Calr, two tumor-suppressing proteins previously identified by our group using mass spectrometry-based whole-genome proteomics analysis.[12,13] In CW CM derived from Jurkat cells, the levels of MSN and Calr were elevated by Western blotting as well as ELISA-based quantification (Fig. 7A, B). While CW CM downregulated Lrp5, Runx 2, and Snail and elevated cleaved caspase 3 in U2OS cells in 1 day (Fig. S6), the application of MSN and Calr recombinant proteins also reduced the levels of Lrp5, Runx2, and Snail with an increase in cleaved caspase 3 in 1 day (Fig. 7C). Consistently, the MTT-based viability and transwell invasion were also inhibited by extracellular MSN and Calr in 2 days (Fig. 7D, E).

Immunoprecipitation of CD91 with calr in RAW264.7 cells, and CD47 with calr in U2OS cells

To assess the potential mechanism of the tumor-suppressive action of Calr, we conducted an immunoprecipitation assay using RAW264.7 pre-osteoclast cells and U2OS cells. Regarding RAW264.7 cells, CD91 was co-immunoprecipitated with Calr (Fig. 7F). Notably, the proliferation of U2OS cells was inhibited by Calr recombinant proteins in the presence of RAW264.7 cells (Fig. 7G, H), and silencing of CD91 in RAW264.7 cells suppressed Calr-driven reduction in MTT-based viability (Fig. 7I), suggesting that the interactions of extracellular Calr with CD91 in RAW264.7 cells is responsible for the anti-tumor action. Regarding U2OS cells, CD47 was co-immunoprecipitated with Calr (Fig. 7J). Silencing CD47 suppressed Calr-driven MTT-based tumor inhibition as well as the downregulation of Lrp5, Runx 2, and Snail in U2OS cells (Fig. 7K, L). Taken together, the result indicates the involvement of CD47 and CD91 in the anti-tumor actions of extracellular Calr.

Suppression of tumorigenic behaviors of patient-derived xenograft (PDX) xenoline (TT2-77) by CW CM

Besides OS cell lines, we examined the anti-tumor effects of CW CM on the patient-derived xenograft (PDX) xenoline (TT2-77). Consistently, CW CM suppressed MTT-based viability, scratch-based migration, EdU-based proliferation, and transwell invasion of TT2-77 cells (Fig. 8A—D).

Discussion

This study presented that the daily administration of PKA-activated lymphocyte-derived CM inhibited the growth of MG63 and U2OS cell lines, as well as PDX OS TT2-77 cells *in vitro* and in the U2OS-colonized mouse tibia *in vivo*. PKA was activated by the pharmacological agent, CW008, as well as cAMP and cAMP analog in Jurkat cells, primary T lymphocytes, and mononuclear cells derived from human peripheral blood samples. CW CM was reproducibly

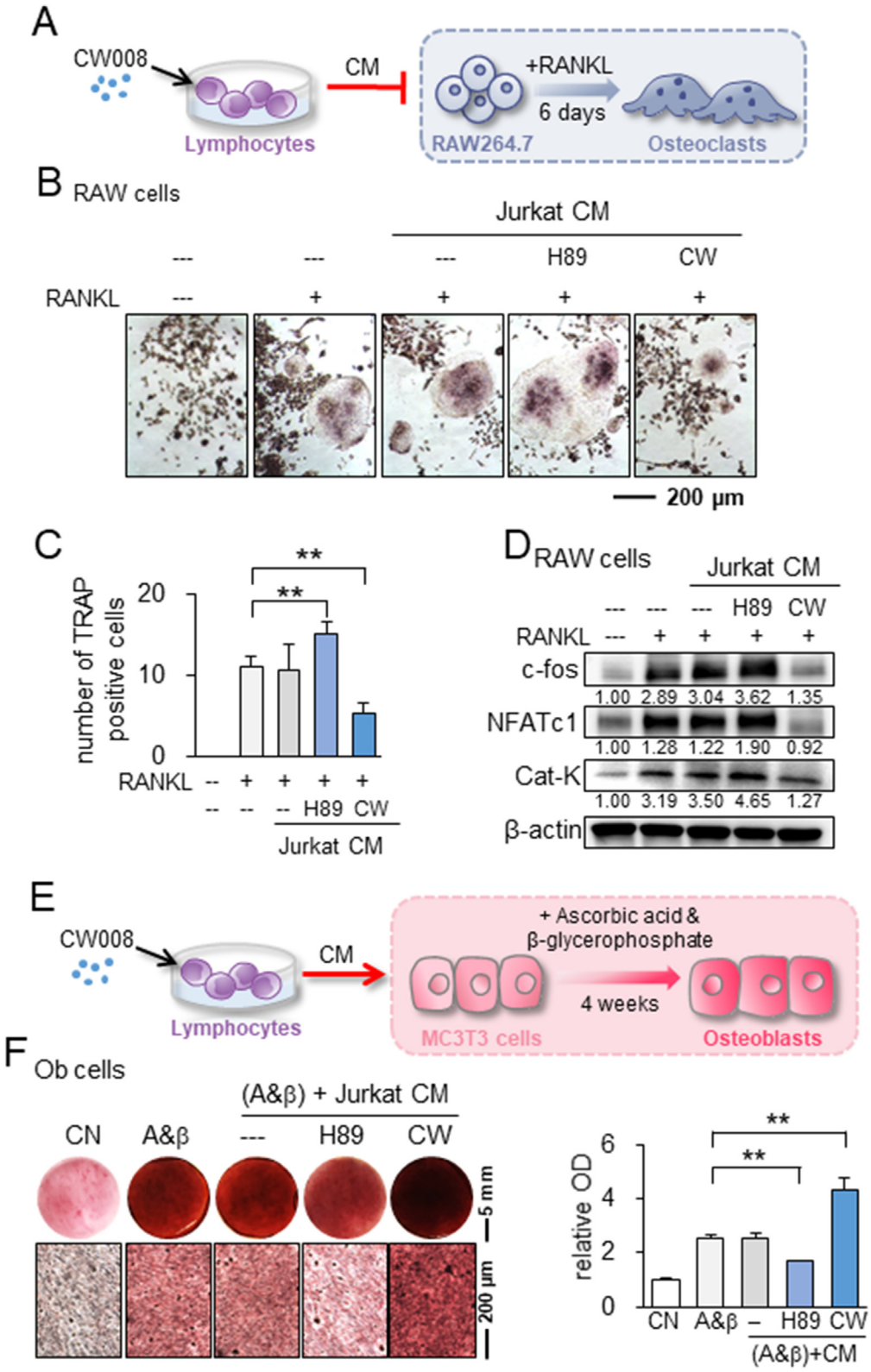

Figure 4 Effect of CW CM and H89 CM on the differentiation of osteoclasts and osteoblasts. CW = CW008, H89 = H89 dihydrochloride, RAW = RAW264.7 cells, Ob = osteoblast, CN = control, CM = conditioned medium, and A&β = ascorbic acid and β-glycerophosphate. The double asterisks indicate $p < 0.01$ **(A)** Schematic illustration of CW CM on the differentiation of osteoclasts. **(B, C)** Trap-staining of RANKL-stimulated RAW264.7 pre-osteoclasts in response to Jurkat CM, H89 CM, and CW CM. **(D)** Upregulation of c-fos, NFATc1, and cathepsin K by H89 CM and their downregulation by CW CM. **(E)** Schematic illustration of CW CM on the differentiation of osteoblasts. **(F)** Enhanced Alizarin-red staining of MC3T3 osteoblasts by CW CM and reduced staining by H89 CM.

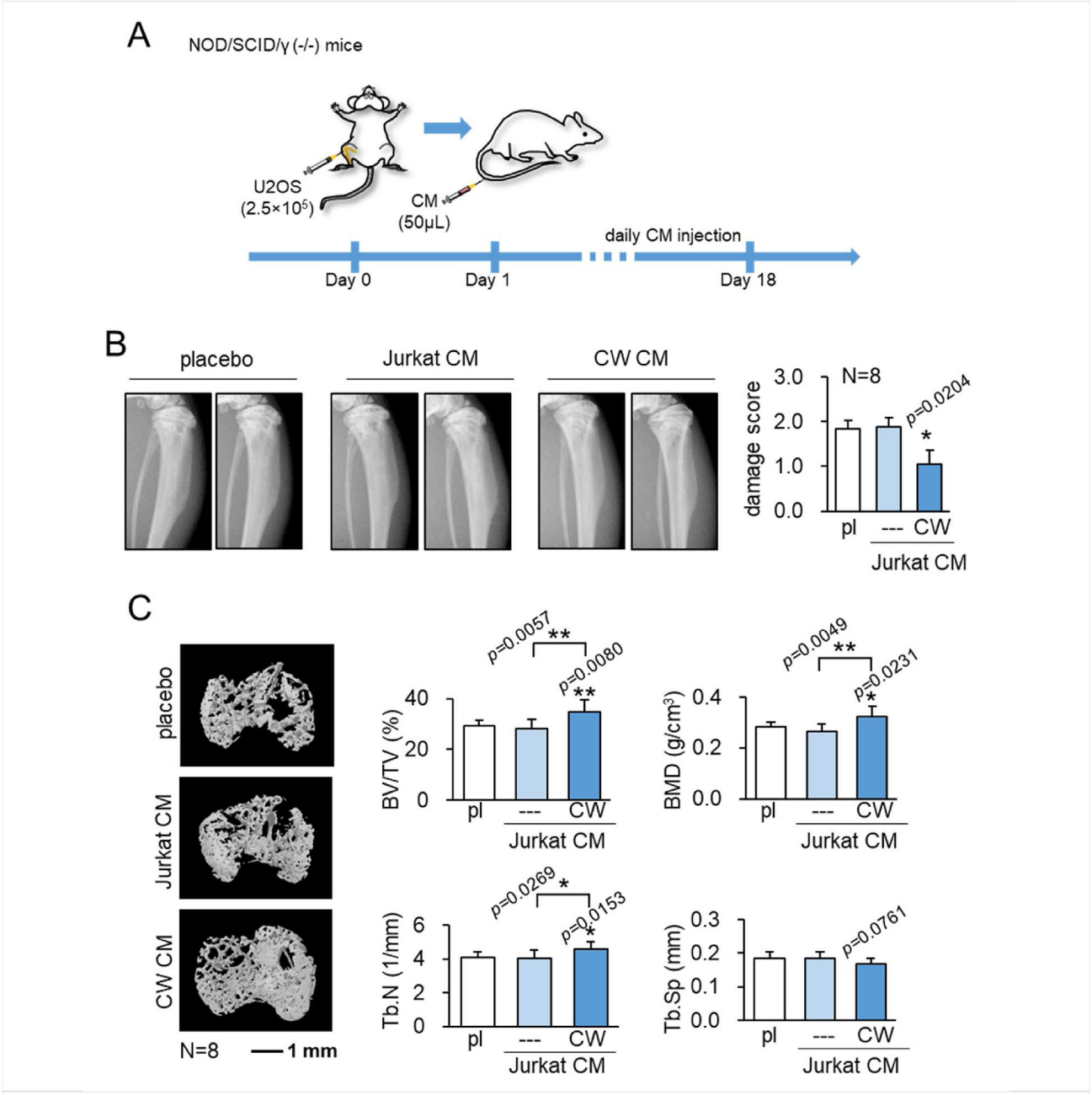

Figure 5 Bone protection *in vivo* by CW008-treated Jurkat cell-derived CM. pl = placebo, CM = conditioned medium, and CW = CW008. The single and double asterisks indicate $P < 0.05$ and 0.01, respectively. **(A)** Timeline of the animal experiment, in which U2OS cells were injected into the tibia of NOD/SCID/γ $(-/-)$ (NSG) female mouse. CW CM was given daily as an intravenous injection to the tail vein from day 1 and mice were sacrificed on day 18. **(B)** Reduction of bone degradation in the tibia of NSG mice by the systemic administration of CW CM. **(C)** Protection of trabecular bone in the tumor-invaded proximal tibia by CW CM. BV/TV = bone volume ratio, BMD = bone mineral density, Tb.N = trabecular number, and Tb. Sp = trabecular separation.

enriched with MSN and Calr, and they acted as extracellular tumor suppressors. Mechanistically, extracellular Calr interacted with CD91, a plasma membrane receptor in the family of low-density lipoprotein receptors, in RAW264.7 macrophages. Calr also interacted with CD47, a transmembrane protein in the immunoglobulin superfamily, in U2OS cells. Both CD91 and CD47 mediated Calr-driven antitumor actions. Besides lymphocytes and blood-derived mononuclear cells, iTSCs were generated from bone cells such as bone marrow-derived MSCs and osteoblasts. In addition to the suppression of tumor progression, CW CM contributed to protecting bone loss by impeding osteoclast differentiation and enhancing osteoblast development (Fig. 8E).

The elimination of OS cells by iTSC proteomes such as that found in CW CM resembles the removal of loser cells nearby winner cells in the organogenesis observed in Drosophila. It is reported that winner cells secrete unknown

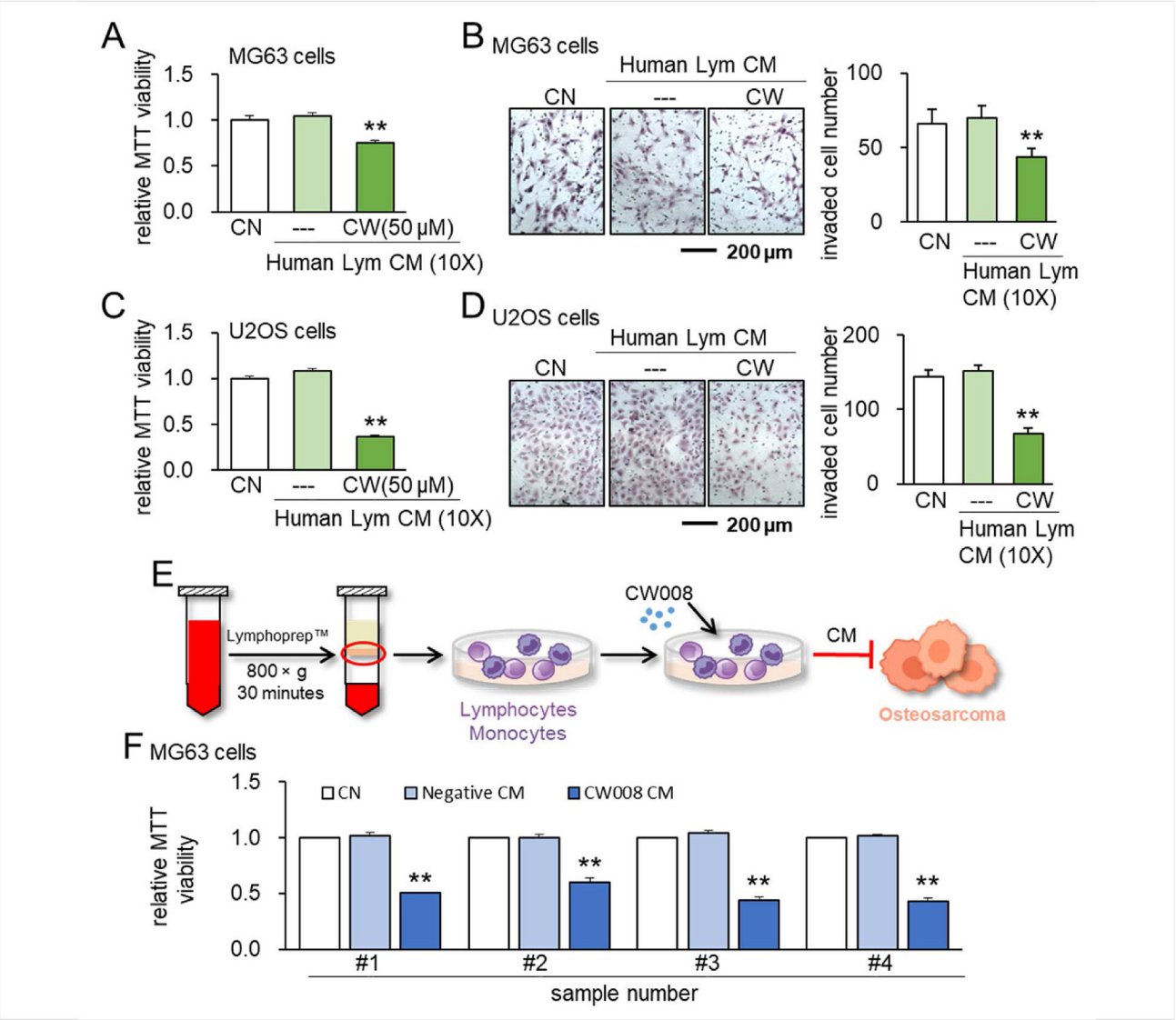

Figure 6 Anti-tumor effects of human lymphocytes-derived and mononuclear cells-derived CM. CN = control, CM = conditioned medium, CW = CW008, and Lym = Lymphocytes. The double asterisks indicate $P < 0.01$. **(A, B)** Reduction in MTT-based viability and transwell invasion of MG63 OS cells by 50 μM CW008-treated human lymphocytes-derived CM. **(C, D)** Reduction in MTT-based viability and transwell invasion of U2OS cells by 50 μM CW008-treated human lymphocytes-derived CM. **(E)** Illustration of the anti-tumor effects of human mononuclear cell-derived CM. **(F)** Anti-tumor effect of 50 μM CW008-treated CM to MG63 CS cells. CM was generated using lymphocytes in 4 human peripheral blood samples. In A to F, CM was condensed by 10 times.

proteins that induce the death of loser cells via JNK signaling.[23] Cell competition has also been reported between Myc-overexpressing cells and wild-type cells in Drosophila and mice, in which Myc-overexpressing cells can kill wild-type cells at a distance.[24,47] Based on the current and previous iTSC studies together with the cell competition in Drosophila and mice, an emerging paradigm for a novel option for cancer treatment is to utilize the competition-driven anti-tumor capability of iTSC CM thereby weakening tumor cells. To reach its full clinical potential, future studies would evaluate whether the existing chemotherapeutic strategy is compatible with the application of iTSC proteomes.

The current study together with our previous iTSC studies shed light on the counterintuitive approach of generating anti-tumor CM and its mechanism for suppressing the progression of OS and other tumors. Bone cells including MSCs, osteoblasts, osteoclasts, and osteocytes can be converted into iTSCs by activating Wnt and PI3K signaling.[10–14] For lymphocytes, the activation of PKA signaling was significantly more effective than the activation of Wnt or PI3K pathways (Fig. S7). These differences highlight the importance of understanding the mechanisms behind the cell type-dependent procedure of iTSC generation. Interestingly, in both PI3K-activated MSC CM and PKA-activated lymphocyte CM, extracellular MSN and Calr were enriched.[12,13] They act as moonlighting proteins, serving as a tumor suppressor extracellularly and a tumor promoter intracellularly. Notably, our previous results indicated that extracellular MSN interacted with a membrane-bound CD44

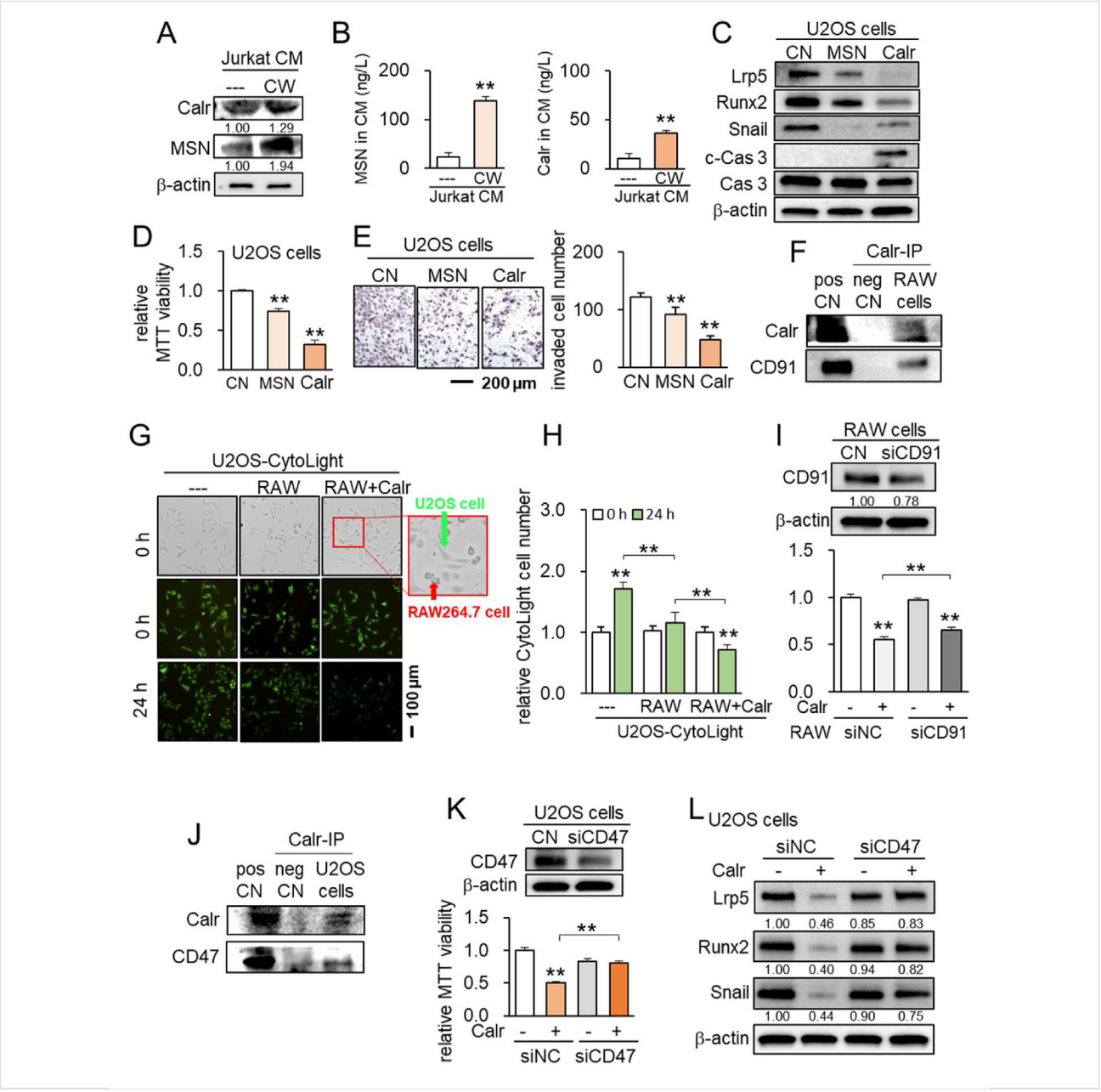

Figure 7 Calreticulin and moesin as tumor-suppressing proteins in CW CM. CN = control, pos CN = positive control, neg CN = negative control, si = siRNA, NC = negative control, CW = CW008, CM = conditioned medium, MSN = moesin, and Calr = Calreticulin. The double asterisk indicates $P < 0.01$. **(A)** Elevation of MSN and Calr in CW CM. **(B)** ELISA-based levels of MSN and Calr in CW CM. **(C)** Reduction in Lrp5, Runx 2, and Snail, as well as an increase in cleaved caspase 3 (c-Cas 3) by MSN and Calr. **(D, E)** Reduction in the MTT-based viability and transwell invasion of U2OS cells by the application of 1 μg/mL MSN and 0.7 μg/mL Calr. **(F)** Co-immunoprecipitation of CD91 with Calr in RAW264.7 cells. **(G, H)** Reduction in U2OS cells by co-culturing with RAW264.7 cells with 0.5 μg/mL Calr. **(I)** Silencing of CD47 in RAW cells suppressed Calr-driven reduction in MTT-based viability of U2SO OS cells. **(J)** Co-immunoprecipitation of CD47 with Calr. **(K)** Suppression of Calr-driven reduction in MTT-based viability of U2OS cells by silencing CD47. **(L)** Silencing of CD47 in U2OS cells suppressed Calr-driven downregulation of Lrp5, Runx2, and Snail.

in tumor cells, and silencing CD44 reduced MSN's anti-tumor effect.[13] Also, it is reported that the overexpression of CD44 enhanced metastatic potential in U2OS cells. In this study, we observed that Calr interacted with CD91, which is expressed in RAW264.7 pre-osteoclasts. It also interacted with CD47, an immunoglobulin, which is overexpressed in many types of cancer cells. Consistent with this, it has been reported that CD47 blockade inhibits tumor progression of human OS in xenograft models.[48] Further studies are recommended to examine whether CW CM in this study shows

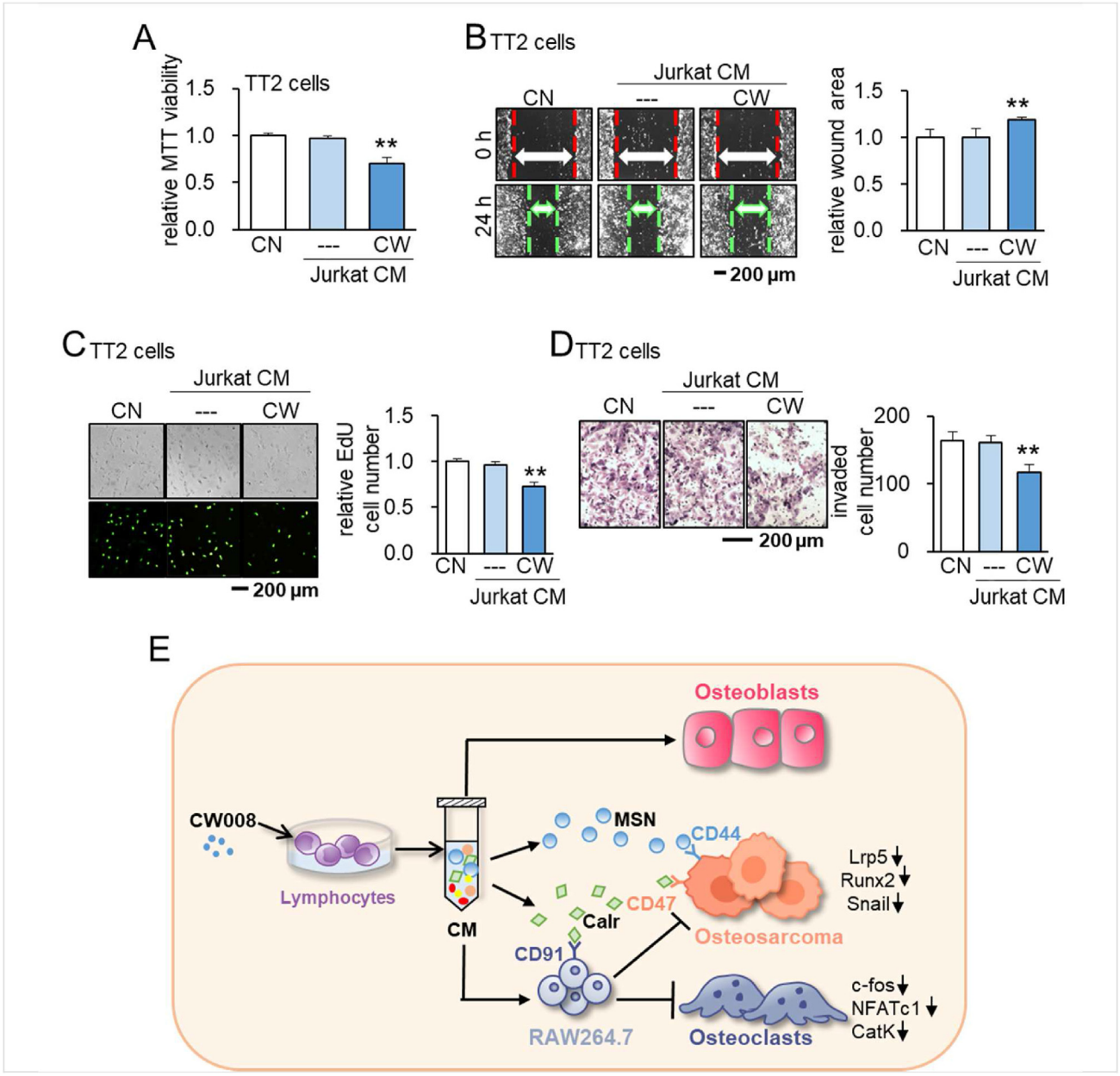

Figure 8 Effects of CW CM on the patient-derived xenograft (PDX) xenoline (TT2-77). CN = control, CW = CW008, and CM = conditioned medium. The double asterisk indicates $P < 0.01$. **(A–D)** Suppression of MTT-based viability, scratch-based migration, EdU-based proliferation, and transwell invasion of TT2 cells by CW008-treated Jurkat cell-derived CM, respectively. **(E)** Schematic diagram for the putative regulatory mechanism of the tumor-suppressing action of CW008-treated lymphocyte-derived CM. CW CM suppresses the progression of OS cells via moesin (MSN) and the calreticulin (Calr)-CD47/CD91 axis. CW CM also alters bone homeostasis by stimulating osteoblast development and impeding osteoclast development.

anti-tumor actions on other cancers such as breast cancer and prostate cancer and whether PKA activation induces iTSCs in other types of cells such as MSCs.

From a translational viewpoint, we chose lymphocytes and mononuclear cells for the generation of iTSCs since they would allow autologous usage of peripheral blood from a patient with OS. We also consider the potential linkage to chimeric antigen receptor (CAR) T cell immunotherapy that employs T cells with transfected chimeric antigen receptors.[49] Since the procedure for applying engineered T cells to cancer patients is established, we may develop T cell-derived iTSCs and proteomes using the CART cell technology. Alternatively, we may examine the possibility of converting CART cells into iTSCs by genetic manipulation or chemical treatment and augmenting the target anti-tumor capability of CART cells.

Although this study presented the striking anti-tumor action of CW CM, there are limitations. First, efficacies of iTSC CM were untested for multiple variants of OS disease types. We employed MG63, osteoblast-like OS cell line, and U2OS, negative for most of the osteoblastic markers,[50] together with PDX OS TT2-77 cells. Second,

while CW008 is known to activate the cAMP/PKA/CEB pathway and stimulate osteogenic differentiation of bone marrow-derived MSCs, its action may not be completely specific to PKA signaling. Third, the secretome from iTSCs includes other molecules such as nucleic acids, small metabolites, lipids, etc. This study focused on proteomes analysis since the treatment with nucleases, a removal of exosomes by ultracentrifugation, and filtering with 3 kD cutoff did not significantly alter the anti-tumor capabilities of CW CM.

Conclusions

The study illustrated an uncommon claim of therapeutic option, in which tumorigenic signaling is stimulated for the development of iTSCs. In addition to existing targets such as angiogenesis, cell cycling, cellular metabolism, etc., we envision that identifying extracellular MSN and Calr as tumor suppressors and predicting their binding partners contributes to expanding the scope of targeted protein therapy. In summary, we demonstrated that lymphocytes and mononuclear cells, obtained from the peripheral blood, can be converted into iTSCs and their proteomes can protect bone from OS without inducing a vicious cycle between OS cells and bone-resorbing osteoclasts. The therapeutic possibilities include the local and global administration of iTSCs and their CM, targeted delivery of a protein cocktail consisting of the selected tumor-suppressing proteins, and the identification of cell-surface receptors as druggable targets that mediate CM's anti-tumor action.

Author contributions

Conception and experimental design: KM, KEP, BYL, HY; Data collection and interpretation: KL, XS, HL, HM, MZ, KM, KT, KO, PHP, MRS, MAK, KEP, BYL, HY; Drafted manuscript: KL, XS, KM, MAK, HY.

Funding

This work was supported by The Biomechanics and Biomaterials Research Center at Indiana University-Purdue University Indianapolis, USA (No. 2201-01); The NIH/Eunice Kennedy Shriver NICHD, USA (No. P50HD090215); The NIH/NCI Cancer Center Support Grant, USA (No. P30CA082709); The Tyler Trent Cancer Research Endowment for the Riley Hospital for Children IU-Health, USA; The Indiana University Grand Challenge—Precision Health Initiative, USA.

Conflict of interests

The authors declare no competing interests.

Abbreviations

BMD	bone mineral density
BV/TV	bone volume ratio
Calr	calreticulin
(CAR) T cell	chimeric antigen receptor T cell
HMGB1	high mobility group box protein 1
iTSCs	induced tumor-suppressing cells
MSN	moesin
NSG	NOD/SCID/γ $(-/-)$
OS	osteosarcoma
PDX	patient-derived xenograft
TRAP	tartrate-resistant acid phosphate
Tb.N	trabecular number
Tb.Sp	trabecular separation

Appendix A. Supplementary data

Supplementary data to this article can be found online at https://doi.org/10.1016/j.gendis.2022.08.007.

References

1. Taran SJ, Taran R, Malipatil NB. Pediatric osteosarcoma: an updated review. *Indian J Med Paediatr Oncol*. 2017;38(1):33—43.
2. Carrle D, Bielack SS. Current strategies of chemotherapy in osteosarcoma. *Int Orthop*. 2006;30(6):445—451.
3. Ferguson WS, Goorin AM. Current treatment of osteosarcoma. *Cancer Invest*. 2001;19(3):292—315.
4. Adamopoulos C, Gargalionis AN, Basdra EK, Papavassiliou AG. Deciphering signaling networks in osteosarcoma pathobiology. *Exp Biol Med (Maywood)*. 2016;241(12):1296—1305.
5. Maeda H, Khatami M. Analyses of repeated failures in cancer therapy for solid tumors: poor tumor-selective drug delivery, low therapeutic efficacy and unsustainable costs. *Clin Transl Med*. 2018;7(1):11.
6. Liu SZ, Sun X, Li KX, et al. Tumor cell secretomes in response to anti- and pro-tumorigenic agents. *Onco*. 2021;1(2):101—113.
7. Roslan Z, Muhamad M, Selvaratnam L, Ab-Rahim S. The roles of low-density lipoprotein receptor-related proteins 5, 6, and 8 in cancer: a review. *J Oncol*. 2019;2019:4536302.
8. Wong KK, Engelman JA, Cantley LC. Targeting the PI3K signaling pathway in cancer. *Curr Opin Genet Dev*. 2010;20(1):87—90.
9. Liu X, Yun F, Shi L, Li ZH, Luo NR, Jia YF. Roles of signaling pathways in the epithelial-mesenchymal transition in cancer. *Asian Pac J Cancer Prev*. 2015;16(15):6201—6206.
10. Liu S, Wu D, Sun X, et al. Overexpression of Lrp5 enhanced the anti-breast cancer effects of osteocytes in bone. *Bone Res*. 2021;9(1):32.
11. Sano T, Sun X, Feng Y, et al. Inhibition of the growth of breast cancer-associated brain tumors by the osteocyte-derived conditioned medium. *Cancers*. 2021;13(5):1061.
12. Sun X, Li K, Zha R, et al. Preventing tumor progression to the bone by induced tumor-suppressing MSCs. *Theranostics*. 2021;11(11):5143—5159.
13. Sun X, Li K, Hase M, et al. Suppression of breast cancer-associated bone loss with osteoblast proteomes via Hsp90ab1/-moesin-mediated inhibition of TGFβ/FN1/CD44 signaling. *Theranostics*. 2022;12(2):929—943.
14. Liu S, Sun X, Li K, et al. Generation of the tumor-suppressive secretome from tumor cells. *Theranostics*. 2021;11(17):8517—8534.
15. Han Y, Li X, Zhang Y, Han Y, Chang F, Ding J. Mesenchymal stem cells for regenerative medicine. *Cells*. 2019;8(8):886.
16. Guedan S, Calderon H, Posey Jr AD, Maus MV. Engineering and design of chimeric antigen receptors. *Mol Ther Methods Clin Dev*. 2019;12:145—156.
17. Roessner A, Lohmann C, Jechorek D. Translational cell biology of highly malignant osteosarcoma. *Pathol Int*. 2021;71(5):291—303.

18. Tung KH, Ernstoff MS, Allen C, Shu S. A review of exosomes and their role in the tumor microenvironment and host-tumor "macroenvironment". *J Immunol Sci*. 2019;3(1):4—8.
19. Madden EC, Gorman AM, Logue SE, Samali A. Tumour cell secretome in chemoresistance and tumour recurrence. *Trends Cancer*. 2020;6(6):489—505.
20. Wu JY, Huang TW, Hsieh YT, et al. Cancer-derived succinate promotes macrophage polarization and cancer metastasis via succinate receptor. *Mol Cell*. 2020;77(2):213—227.
21. Cebrián MJ, Bauden M, Andersson R, Holdenrieder S, Ansari D. Paradoxical role of HMGB1 in pancreatic cancer: tumor suppressor or tumor promoter? *Anticancer Res*. 2016;36(9): 4381—4389.
22. Obenauf AC, Zou Y, Ji AL, et al. Therapy-induced tumour secretomes promote resistance and tumour progression. *Nature*. 2015;520(7547):368—372.
23. Nagata R, Nakamura M, Sanaki Y, Igaki T. Cell competition is driven by autophagy. *Dev Cell*. 2019;51(1):99—112.
24. Clavería C, Giovinazzo G, Sierra R, Torres M. Myc-driven endogenous cell competition in the early mammalian embryo. *Nature*. 2013;500(7460):39—44.
25. Kajita M, Fujita Y. EDAC: epithelial defence against cancer-cell competition between normal and transformed epithelial cells in mammals. *J Biochem*. 2015;158(1):15—23.
26. Fouad YA, Aanei C. Revisiting the hallmarks of cancer. *Am J Cancer Res*. 2017;7(5):1016—1036.
27. Zhang H, Kong Q, Wang J, Jiang Y, Hua H. Complex roles of cAMP-PKA-CREB signaling in cancer. *Exp Hematol Oncol*. 2020; 9(1):32.
28. Delghandi MP, Johannessen M, Moens U. The cAMP signalling pathway activates CREB through PKA, p38 and MSK1 in NIH 3T3 cells. *Cell Signal*. 2005;17(11):1343—1351.
29. Barros FBA, Assao A, Garcia NG, et al. Moesin expression by tumor cells is an unfavorable prognostic biomarker for oral cancer. *BMC Cancer*. 2018;18(1):53.
30. Schcolnik-Cabrera A, Oldak B, Juárez M, Cruz-Rivera M, Flisser A, Mendlovic F. Calreticulin in phagocytosis and cancer: opposite roles in immune response outcomes. *Apoptosis*. 2019; 24(3—4):245—255.
31. Mayr L, Pirker C, Lötsch D, et al. CD44 drives aggressiveness and chemoresistance of a metastatic human osteosarcoma xenograft model. *Oncotarget*. 2017;8(69):114095—114108.
32. Wiersma VR, Michalak M, Abdullah TM, Bremer E, Eggleton P. Mechanisms of translocation of ER chaperones to the cell surface and immunomodulatory roles in cancer and autoimmunity. *Front Oncol*. 2015;5:7.
33. Chen Q, Fang X, Jiang C, Yao N, Fang X. Thrombospondin promoted anti-tumor of adenovirus-mediated calreticulin in breast cancer: relationship with anti-CD47. *Biomed Pharmacother*. 2015;73:109—115.
34. Takigawa S, Chen A, Nishimura A, et al. Guanabenz downregulates inflammatory responses via eIF2α dependent and independent signaling. *Int J Mol Sci*. 2016;17(5):674.
35. Stenson WF, Nickells MW, Atkinson JP. Metabolism of exogenous arachidonic acid by murine macrophage-like tumor cell lines. *Prostaglandins*. 1981;21(5):675—689.
36. Pandya PH, Cheng L, Saadatzadeh MR, et al. Systems biology approach identifies prognostic signatures of poor overall survival and guides the prioritization of novel BET-CHK1 combination therapy for osteosarcoma. *Cancers*. 2020;12(9):2426.
37. Kim JM, Choi JS, Kim YH, et al. An activator of the cAMP/P-KA/CREB pathway promotes osteogenesis from human mesenchymal stem cells. *J Cell Physiol*. 2013;228(3):617—626.
38. Jahchan NS, Dudley JT, Mazur PK, et al. A drug repositioning approach identifies tricyclic antidepressants as inhibitors of small cell lung cancer and other neuroendocrine tumors. *Cancer Discov*. 2013;3(12):1364—1377.
39. Li F, Chen A, Reeser A, et al. Vinculin force sensor detects tumor-osteocyte interactions. *Sci Rep*. 2019;9(1):5615.
40. Oh YS, Kim HY, Song IC, et al. Hypoxia induces CXCR4 expression and biological activity in gastric cancer cells through activation of hypoxia-inducible factor-1α. *Oncol Rep*. 2012; 28(6):2239—2246.
41. Takigawa S, Frondorf B, Liu S, et al. Salubrinal improves mechanical properties of the femur in osteogenesis imperfecta mice. *J Pharmacol Sci*. 2016;132(2):154—161.
42. Zeng XZ, He LG, Wang S, et al. Aconine inhibits RANKL-induced osteoclast differentiation in RAW264.7 cells by suppressing NF-κB and NFATc1 activation and DC-STAMP expression. *Acta Pharmacol Sin*. 2016;37(2):255—263.
43. Hwang PW, Horton JA. Variable osteogenic performance of MC3T3-E1 subclones impacts their utility as models of osteoblast biology. *Sci Rep*. 2019;9(1):8299.
44. Bonar SL, Brydges SD, Mueller JL, et al. Constitutively activated NLRP3 inflammasome causes inflammation and abnormal skeletal development in mice. *PLoS One*. 2012;7(4):e35979.
45. Bouxsein ML, Boyd SK, Christiansen BA, Guldberg RE, Jepsen KJ, Müller R. Guidelines for assessment of bone microstructure in rodents using micro-computed tomography. *J Bone Miner Res*. 2010;25(7):1468—1486.
46. Liu S, Fan Y, Chen A, et al. Osteocyte-driven downregulation of Snail restrains effects of Drd2 inhibitors on mammary tumor cells. *Cancer Res*. 2018;78(14):3865—3876.
47. Amoyel M, Bach EA. Cell competition: how to eliminate your neighbours. *Development*. 2014;141(5):988—1000.
48. Xu JF, Pan XH, Zhang SJ, et al. CD47 blockade inhibits tumor progression human osteosarcoma in xenograft models. *Oncotarget*. 2015;6(27):23662—23670.
49. Feins S, Kong W, Williams EF, Milone MC, Fraietta JA. An introduction to chimeric antigen receptor (CAR) T-cell immunotherapy for human cancer. *Am J Hematol*. 2019;94(S1): S3—S9.
50. Pautke C, Schieker M, Tischer T, et al. Characterization of osteosarcoma cell lines MG-63, Saos-2 and U-2 OS in comparison to human osteoblasts. *Anticancer Res*. 2004;24(6): 3743—3748.